

Monoclinic to tetragonal transformations in hafnia and zirconia: A combined calorimetric and density functional study

Xuhui Luo,¹ Wei Zhou,² Sergey V. Ushakov,² Alexandra Navrotsky,² and Alexander A. Demkov^{1,*}

¹*Department of Physics, The University of Texas, Austin, Texas 78712, USA*

²*Environmental Materials Chemistry Peter A Rock Thermochemistry Laboratory, University of California, Davis, California 95616, USA*

(Received 10 August 2009; revised manuscript received 28 September 2009; published 21 October 2009)

We use a combination of density functional theory and calorimetric measurements to investigate the monoclinic to tetragonal transition in hafnia and zirconia. We measure the transition enthalpies to be 8.4 ± 0.7 kJ/mol in hafnia and, as previously reported, 5.272 ± 0.544 kJ/mol in zirconia. Calculated values are 10.21 and 7.50 kJ/mol for hafnia and zirconia, respectively. We formulate a theoretical model of the phase transition consistent with the martensitic character of the transformations. The transition barriers of 20.3 and 16.3 kJ/mol are estimated for hafnia and zirconia, respectively. We report the phonon spectra of monoclinic and tetragonal phases of both oxides and identify the Raman and IR active modes. The theoretical results compare well with available experiments. We present a comprehensive theoretical comparison of thermodynamic properties of zirconia and hafnia including the temperature dependence of specific heat.

DOI: [10.1103/PhysRevB.80.134119](https://doi.org/10.1103/PhysRevB.80.134119)

PACS number(s): 64.60.-i, 63.20.dk, 65.40.Ba

I. INTRODUCTION

In recent years, both hafnia and zirconia have been looked at closely in the quest for a high permittivity gate dielectric to replace silicon oxide in advanced metal oxide semiconductor field effect transistors.^{1,2} Hafnium dioxide or HfO_2 is chosen for its high dielectric constant (five times that of SiO_2) and compatibility with stringent requirements of the Si process. As deposited, thin hafnia films are typically amorphous but crystallize after a postdeposition anneal.³ Though thermodynamic properties of thin film may differ from those of bulk samples⁴ understanding of bulk thermodynamics is a first step. Bulk crystalline hafnia and zirconia both undergo a succession of phase transitions from the high temperature high symmetry cubic phase [space group $Fm\bar{3}m$; see Fig. 1(a)] to slightly distorted structures with tetragonal [space group $P4_2/nmc$; see Fig. 1(b)] and monoclinic [space group $P2_1/c$; Fig. 1(c)] symmetries. Unlike four-coordinated silicon in the (4,2) tetrahedral framework of SiO_2 ,⁵ hafnium in HfO_2 maintains a relatively high coordination presumably even in the amorphous phase.⁶ The transition temperatures of the cubic to tetragonal transition are about 2900 K (Ref. 7) for hafnia and 2600 K (Ref. 8) for zirconia. Experimental data on the monoclinic to tetragonal (MT) transformation in ZrO_2 are readily available.⁹⁻¹² The transition shows considerable hysteresis and some dependence on sample preparation, occurring at 1420–1478 K for ZrO_2 on heating and 1273–1325 K on cooling.¹⁰ Moriya and Navrotsky¹¹ reported the transition enthalpy of 5.43 ± 0.31 kJ/mol and entropy of 3.69 ± 0.21 J/(mol K)⁻¹. The axial thermal expansion of ZrO_2 over the temperature range from 298 to 1673 K has been studied by Patil and Subbarao.¹² They reported a 3.0% volume contraction during the transformation at 1427 K. Because of the higher transition temperature, experimental data on the MT transformation of HfO_2 are more limited. High temperature x-ray diffraction analysis has been the main technique used to determine the transformation temperature.^{13,14}

We have not found any reports of direct measurement of the enthalpy of the MT or the tetragonal to cubic (TC) trans-

formations in hafnia. Schick¹⁵ and Barin *et al.*¹⁶ estimated the transformation enthalpy to be 10.46 kJ/mol at 1973 K by combining Orr's¹⁷ heat content data below 1973 K and Pears'¹⁸ data above 1973 K. Wang *et al.*¹⁰ calculated the enthalpy of the MT transformation to be 8.21 kJ/mol by adopting the same entropy of transformation as for ZrO_2 and a MT transition temperature of 2052 K.

In recent years the crystallographic structures, vibrational and electronic spectra, and dielectric constants of bulk hafnia and zirconia have been studied theoretically.¹⁹⁻²⁴ However, theoretical analysis of the phase transitions in both materials is at best incomplete. There is a comprehensive theoretical

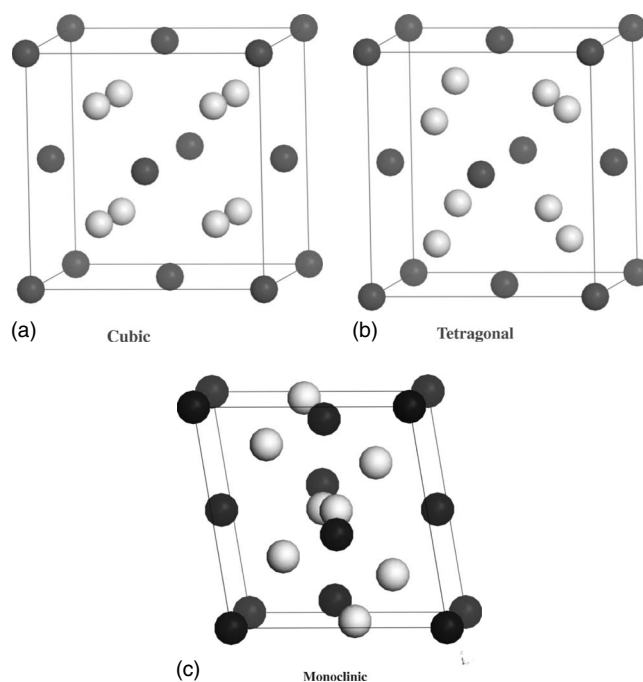


FIG. 1. Structures of three HfO_2 phases. Black balls and white balls denote Hf and O atoms, respectively.

study of high pressure phase transitions in ZrO_2 done by Ozturk and Durandurdu.²⁵

In this paper we report a joint theoretical and experimental study of the monoclinic to tetragonal phase transformations in hafnia and zirconia. We measure the transition temperature, the volume change, and the enthalpy of the transformation in hafnia using differential thermal analysis (DTA) and thermomechanical analysis. Using density functional theory (DFT) we investigate the MT phase transition by calculating the potential energy surface (PES) and allowing for a change of both the lattice cell vectors and internal coordinates. We calculate the enthalpy, entropy, and temperature of the transition as well as the heat capacity of the monoclinic and tetragonal phases. Using transition state theory we identify the minimum energy path (MEP) for the MT transition. We provide a comprehensive comparison of the structure, thermodynamics, and phonon spectra of hafnia and zirconia.

II. EXPERIMENTAL METHODS

HfO_2 from Alfa Aesar and Aldrich with 99.95% Hf and <0.5% Zr (metal basis) was used for measurements. A Setaram Setsys 2400 instrument (Setaram, Inc., Caluire, France) was used to measure the enthalpy of the MT phase transition in HfO_2 and for dilatometry. A Setaram DTA sensor with W/WRe26 thermocouples for DTA signal and W5Re/W26Re thermocouples for sample and furnace temperature was used with 83 μL tungsten crucibles with lids. Identical crucibles were used for sensitivity calibration with gold and Al_2O_3 melting. Temperature and sensitivity calibration were performed in tungsten crucibles with gold and Al_2O_3 melting. Changes in sensitivity and temperature calibrations due to sensor aging were estimated by repeating calibrations with alumina melting.

Experiments were performed in argon and helium flow using three different sensors. Sensors and furnace thermocouples were rebuilt with tungsten wires with 5% and 26% Re from Rhenium Alloys, Inc., (Elyria, OH). The sensor plates (99.93% tungsten) were reused or ordered from Setaram. The results did not vary systematically with sensor, heating rate, or gas type. Two experiments were performed with additional temperature registration using ratio pyrometers. For these experiments, furnace thermocouple was removed and replaced with custom made flange with fused silica window. Two-color radiation thermometers Mirage OR manufactured by Ircon (Niles, IL) operating in a spectral region of 0.70–1.08 μm with single lens reflex focusing and fiber optic IR-2P unit manufactured by Omega (Stamford, CT) operating at 0.4–1.4 μm with laser-assisted focusing were used in separate experiments. The pyrometers were aimed at the bottom of the sample holder and temperature offset was calibrated by melting alumina.

Dilatometry experiments were performed on the same Setsys 2400 instrument using a graphite probe and sample holder. A HfO_2 pellet 2.5 mm in length and 5 mm in diameter was sintered at 1973 K for 2 h. An electromagnetic load of 5 g was applied and heating and cooling traces were recorded at 10 K/min.

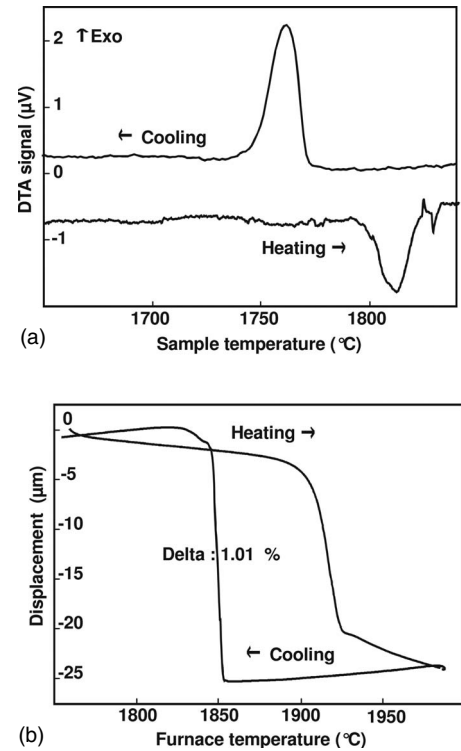


FIG. 2. (a) Differential heat flow traces of HfO_2 . Heating rate at 10 K/min and cooling rate at 20 K/min. Baseline correction applied. (b) Displacement trace for HfO_2 pellet. Heating and cooling rates are 10 K/min. 5 g load. No corrections applied.

III. COMPUTATIONAL METHODOLOGY

DFT calculations within the local density approximation (LDA) were carried out using the Vienna *ab initio* Simulation Package (VASP).²⁶ We employed the projector-augmented wave pseudopotentials.²⁷ For Hf we included 5*d* and 6*s* electrons and for Zr we included 4*d* and 5*s* electrons, while 2*s* and 2*p* electrons were included for oxygen. The Brillouin zone (BZ) integration was performed with the Monkhorst-Pack method²⁸ using a $8 \times 8 \times 8$ special *k*-point grid for both monoclinic and tetragonal simulation cells. The kinetic energy cutoff of 800 eV was found to ensure the total energy convergence to 10^{-6} eV/atom (10^{-4} kJ/mol). The full structural relaxation was performed until the Hellmann-Feynman forces are less than 0.04 eV/Å.

Free energy of the monoclinic and tetragonal phases was calculated within the harmonic approximation. The heat capacity and entropy were calculated by integrating the phonon density of states. Thus these thermodynamic parameters referred to constant volume conditions. The Hellmann-Feynman forces were calculated with the 800 eV energy cutoff and $4 \times 4 \times 4$ *k*-point grid for the supercell and were converged to 10^{-3} eV/Å.

IV. EXPERIMENTAL RESULTS FOR HfO_2

An example of differential heat flow and displacement scans for HfO_2 is given in Fig. 2. The MT transition enthalpy is 8.4 ± 0.7 kJ/mol as an average of 14 measurements (see

TABLE I. Experimental results on monoclinic-tetragonal phase transition in HfO₂. As, Ms—transition onsets on heating and cooling.

Sensor, atmosphere	<i>M</i> (mg)	Expt.	<i>dT/dt</i> (K/min)	As (K)	Ms (K)	<i>T</i> ₀ (K)	ΔH ($\mu\text{V s/g}$)	Sens ($\mu\text{V/W}$)	ΔH (kJ/mol)	
Sensor 1, argon	205.71	First	10	2101			483	15.0	6.8	
			-10		2074	2082	571	15.6	7.7	
		Second	10	2110			662	15.0	9.3	
			-20		2062	2086	539	15.6	7.3	
		Third	10	2110			655	15.0	9.2	
			-20		2067	2089	622	15.6	8.4	
Sensor 2, helium	90.12	First	10	2093 ^a			1115	26.8	8.8	
			-10		2049	2071	1153	27.6	8.8	
	77.43	First	10	2091 ^b			1579	34.9 ^c	9.5	
			-10		2045	2068	1316	36.0	7.7	
	Sensor 3, argon	74.54	First	10	2094			551	17.1	6.8
				-10		2055	2074	819	17.8	9.7
		Second	10	2093			735	17.1	9.1	
			-10		2055	2074	724	17.8	8.6	
Average					<i>T</i> ₀ =2073 ± 10 K		$\Delta H=8.4 \pm 0.7$ kJ/mol			

^aSample temperature measured with Ircom pyrometer, 2104 K.

^bSample temperature measured with Omega pyrometer, 2087 K.

^cThermocouple calibration and sensitivity were adjusted for aging from experiments with Al₂O₃ melting.

Tables I and II) with uncertainty given as two standard deviations of the mean. The As and Ms temperatures in Table I correspond to transformation onsets on heating and on cooling. The hysteresis loop from DTA measurements varies from 311 to 321 K. This value is much smaller than for zirconia and consistent with previous studies.⁴⁸ The equilibrium temperature (where $\Delta G_{\text{MT}}=0$) can be estimated for this martensitic transformation as an average of transformation onsets on heating and on cooling. Taking into account uncertainties in calibration and thermocouple drift, from our experiments *T*₀ can be estimated as 2073 ± 10 K. This temperature is somewhat higher than previously reported.⁴⁸ This difference can be attributed to the effect of carbon from the vitreous carbon furnace protection tube. This provides a reducing atmosphere which may render the hafnia substoichiometric or even produce carbide phases. Such contamination is unavoidable in this instrument.

Dilatometry experiments indicated a volume decrease on the order of 3% on MT transformation, consistent with previous reports from high temperature x-ray diffraction.⁴⁸ It was not possible to retrieve accurate data on volume change on transition and thermal expansion coefficients from dilatometry experiments due to reaction of HfO₂ with the graphite probe. Hafnium carbide, HfC, was identified by powder x-ray diffraction of the sample after dilatometry.

V. COMPUTATIONAL RESULTS

Table III presents the optimized structural parameters for monoclinic and tetragonal polymorphs of HfO₂ and ZrO₂ along with the experimental data. We compare calculated metal-oxygen bond distances with corresponding experimen-

tal values in Table IV. The bonds are labeled as in Fig. 3 showing the MO₇ coordination polyhedron of the monoclinic phase. Overall the agreement is fair with the worst deviation of 3% for the Ib bond in hafnia. The energy (enthalpy) differences between phases are summarized in Table II. Our calculations correctly reproduce the energetic ordering of the phases, increasing in energy from monoclinic to tetragonal to cubic. Because the calculations give us the ground state of a system at zero temperature, the theoretical volume is smaller than the experimental value at room temperature.^{49,50} The generalized gradient approximation (GGA) often gives lattice constants in closer agreement with experiment.⁴⁶ However, the phonon frequencies calculated with the LDA are better than those computed with GGA when calculating the phonons in hafnia and zirconia.¹⁹ In principle, the lattice constant calculated at 0 K should be smaller than that measured at room temperature, and the phonon frequencies should be higher (due to the same unharmonicity that causes thermal expansion). We find that in this case the LDA gives us an overall better description of hafnia and zirconia. Because the enthalpy of a phase transition is equal to the difference in total energy between two phases (the *PΔV* term relating energy and entropy being negligible at atmospheric pressure), we can directly compare the experimental measurements of the enthalpy and theoretical total energy as shown in Table II. The agreement is rather good for both HfO₂ and ZrO₂.

VI. PHONONS, HEAT CAPACITY, AND TRANSITION TEMPERATURE

The heat capacity of monoclinic zirconia is well known from cryogenic to high temperatures,^{51–55} providing a reli-

TABLE II. Phase transition data for ZrO₂ and HfO₂ (M, monoclinic; T, tetragonal; and C, cubic).

Transition		T (K)	ΔH (kJ/mol)	ΔS (J/mol K)	Experimental method and reference	
ZrO ₂	MT	1478	5.941	4	Drop calorimetry (Ref. 29)	
		1475	5.3 ± 0.5	3.56	Calorimetry (Ref. 30)	
		1420	7.763		Calorimetry by mixture method (Ref. 31)	
		1423	8.297	5.836	Calorimetry by mixture method (Ref. 32)	
		1395	5.64	4.07	DSC (Ref. 33)	
		1435	5.2 ± 0.6		DSC (Ref. 34)	
		1286	4.313		DSC (Ref. 35)	
		1478	5.941		Assessed (Ref. 36)	
		1454	6.024		Optimization (Ref. 37)	
		1476	6.441		Optimization (Ref. 38)	
		1478	5.941		Optimization (Ref. 39)	
		1387	6.00		Optimization (Ref. 40)	
		1470	5.4 ± 0.3	3.7 ± 0.2	Transposed temperature drop calorimetry (Ref. 11)	
		1443	10.6	7.3	Extrapolated from solution calorimetry results (Ref. 41)	
	1560	7.5		Theoretical calculation (this work)		
	TC			1.45		Molecular dynamics (Ref. 42)
		2650	5.564	2.09		Assessed (Ref. 36)
		2642	5.968			Optimization (Ref. 37)
		2627	21.699			Optimization (Ref. 38)
		2641	6.045			Optimization (Ref. 39)
2647		7.5			Optimization (Ref. 40)	
2311		3.4 ± 2.1	1.3 ± 0.8		DTA (Ref. 43)	
MC	298	13.5 ± 2.2			Extrapolated from solution calorimetry results (Ref. 44)	
	298	9.7 ± 1.1			Extrapolated from solution calorimetry results (Ref. 45)	
		14.26			theoretical calculation (this work)	
HfO ₂	MT	2052	8.208		Optimization (Ref. 10)	
		1973	10.46		Optimization (Ref. 15)	
		2078	7.7 ± 0.6		DTA (this work)	
		1920	10.21		Theoretical calculation (this work)	
	TC	3073	11.212		Optimization (Ref. 10)	
	MC	298	~30–50			Extrapolated from solution calorimetry results (Ref. 46)
		298	32.5 ± 1.7			Extrapolated from solution calorimetry results (Ref. 47)
			18.11			Theoretical calculation (this work)

able value for its standard entropy at 298 K as well as at higher and lower temperatures. Heat capacity data for monoclinic hafnia are meager and old. Low temperature heat capacity from 52.47 to 298.16 K was measured by Todd⁴⁸ and enthalpy increments of HfO₂ at 382.7–1803.6 K were studied by Orr.¹⁷ Values of heat capacity and standard entropy for tetragonal and cubic phases cannot be obtained directly by C_p measurements because these phases cannot be maintained below their transition temperatures. Thus theoretical calculations for these phases not only can be benchmarked by the data for monoclinic zirconia but also can provide valuable data for tetragonal and cubic zirconia and for all three hafnia polymorphs. The calculated entropies for the MT and TC transitions can then be compared with those

obtained from the measured phase transition enthalpies and temperatures.

First we calculate the phonon dispersion for tetragonal and monoclinic phases of hafnia and zirconia. The short-range force constant matrix is computed in the 96-atom $2 \times 2 \times 2$ supercell (one can choose 12-atom unit cells for both polymorphs; see Sec. VII). To calculate the force constant matrix each atom is displaced in turn along each Cartesian axis by ± 0.04 Å, and the numerical derivative of the force is calculated and averaged to eliminate the odd power unharmonicity. The dynamical matrix is then computed by the usual lattice Fourier transform. Because hafnia is an ionic compound, one needs to consider the long-range Coulomb contributions (particularly at the Γ point).

TABLE III. Theoretical structural parameters for the HfO₂ and ZrO₂ polymorphs in comparison with experimental data.

	<i>a</i> (Å)	<i>b</i> (Å)	<i>c</i> (Å)	<i>β</i> (deg)	Data type and reference
Monoclinic HfO ₂	5.1156	5.1722	5.2948	99.18	Experiment from Ref. 46
	5.119	5.169	5.290	99.25	Experiment from Ref. 47
	5.117	5.172	5.284	99.37	Experiment from Ref. 48
	5.029	5.132	5.183	99.48	Theory from present work
	5.106	5.165	5.281	99.35	Theory from Ref. 6
Monoclinic ZrO ₂	5.156	5.191	5.304	98.9	Experiment from Ref. 49
	5.145	5.208	5.311	99.23	Experiment from Ref. 50
	5.115	5.23	5.26	99.61	Theory from present work
	5.1065	5.1678	5.2700	99.21	Theory from Ref. 19
Tetragonal HfO ₂	5.14		5.25		Experiment from Ref. 51
	5.150		5.295(1760)		Experiment from Ref. 52
	5.175		5.325(2000)		Experiment from Ref. 53
	4.98		5.07		Theory from present work
	5.056		5.127		Theory from Ref. 6
Tetragonal ZrO ₂	5.0282		5.0987		Theory from Ref. 19
	5.07		5.14		Theory from present work
	5.094		5.177		Experiment from Ref. 46

The long-range part of the dynamical matrix is given by⁵⁶

$$\mathbf{D}_{\alpha,\beta}^{long}(\mathbf{k}; \mu\nu) = \frac{4\pi e^2}{V\epsilon_\infty \sqrt{M_\mu M_\nu}} \frac{[\mathbf{k} \cdot \mathbf{Z}^*(\mu)]_\alpha [\mathbf{k} \cdot \mathbf{Z}^*(\nu)]_\beta}{|\mathbf{k}|^2} \times \exp\{-2\pi i \mathbf{g} \cdot [\mathbf{r}(\mu) - \mathbf{r}(\nu)]\} \exp(-\mathbf{k}^2/\rho^2). \quad (1)$$

Here, ρ is a parameter to control the range of the long-range term. We choose $\rho=0.06 \text{ \AA}^{-1}$ and $\epsilon_\infty=5$.¹⁹ We use the Born

 TABLE IV. Experimental and theoretical bond lengths for the HfO₂ and ZrO₂ polymorphs. Ia-Ic and IIa-IId refer to oxygen atoms shown in Fig. 3.

	Experiment for Hf-O distance (Å)	Experiment for Zr-O distance (Å)	Theory for Hf-O distance (Å)	Theory for Zr-O distance (Å)
Ia	2.031	2.057	2.024	2.063
Ib	2.174	2.163	2.111	2.163
Ic	2.052	2.051	2.025	2.058
IIa	2.17	2.189	2.143	2.181
IIb	2.162	2.22	2.114	2.223
IIe	2.202	2.151	2.187	2.146
IIId	2.254	2.285	2.189	2.230

effective charge tensors recently calculated by Zhao and Vanderbilt,¹⁹

$$\mathbf{Z}_{\text{Hf}}^* = \begin{pmatrix} 5.56 & -0.47 & 0.96 \\ -0.13 & 5.55 & 0.14 \\ 0.21 & 0.41 & 4.74 \end{pmatrix},$$

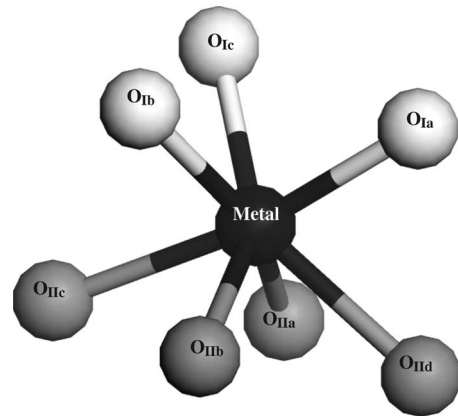


FIG. 3. The configuration of oxygen atoms in the ZrO₇ and HfO₇ polyhedra in ZrO₂ and HfO₂. Three of seven oxygen atoms are threefold coordinated (atoms of type I) and four of them are fourfold coordinated (atoms of type II).

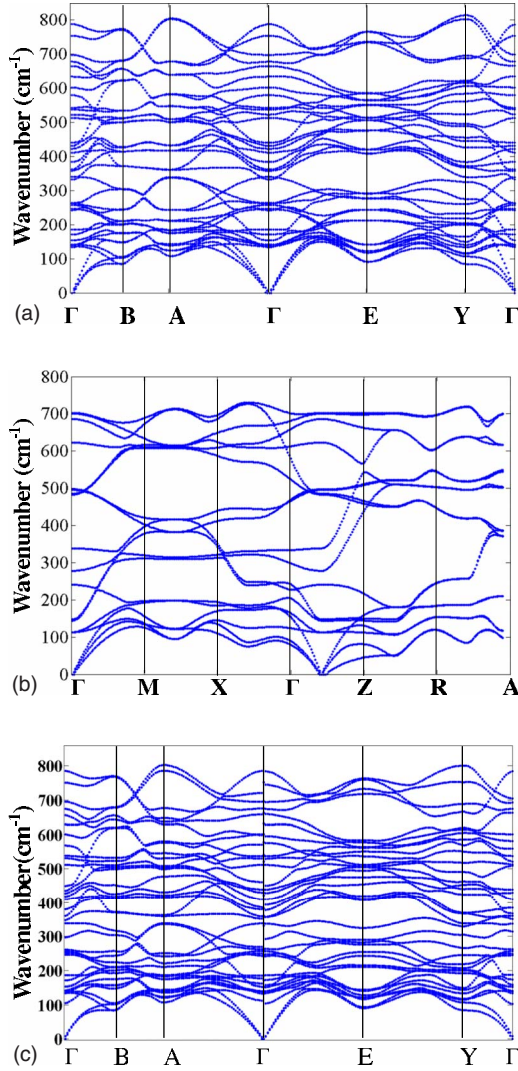


FIG. 4. (Color online) (a) The calculated phonon dispersion of monoclinic hafnia without the long range interactions. (b) The phonon dispersion of tetragonal hafnia without the long range interactions. (c) The phonon dispersion of monoclinic hafnia with long range interactions.

$$Z_{O1}^* = \begin{pmatrix} -3.09 & 0.97 & -0.58 \\ 1.37 & -2.73 & -0.71 \\ -0.18 & -0.61 & -2.24 \end{pmatrix},$$

$$Z_{O2}^* = \begin{pmatrix} -2.48 & 0.20 & -0.39 \\ 0.21 & -2.82 & 0.35 \\ -0.07 & 0.42 & -2.58 \end{pmatrix}.$$

Figures 4(a) and 4(b) show the phonon spectra of monoclinic and tetragonal hafnia calculated including only the short-range contributions to the dynamical matrix. The phonon dispersion is plotted along the high symmetry directions in the first BZ. The path of the calculation for the monoclinic phase starts and ends at the $\Gamma(0,0,0)$ point, going through $B(0,0,\frac{\pi}{a})$, $A(\frac{\pi}{a},0,\frac{\pi}{a})$, Γ , $E(\frac{\pi}{a},\frac{\pi}{a},\frac{\pi}{a})$, and $Y(\frac{\pi}{a},0,0)$, as shown in Fig. 4(a). For the tetragonal phase we start at the Γ point

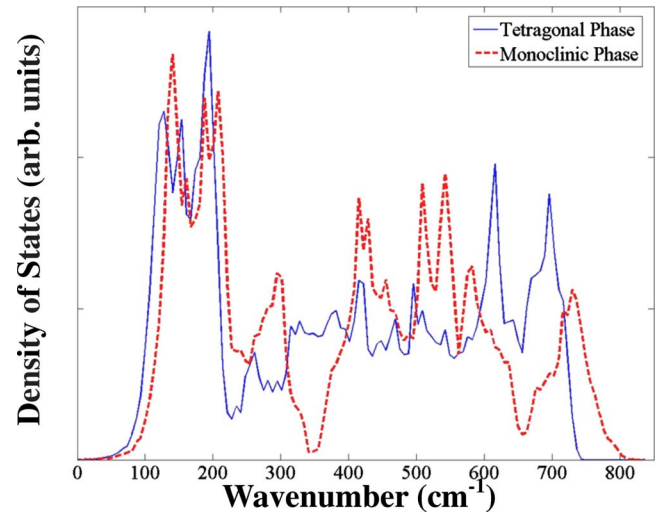


FIG. 5. (Color online) The phonon densities of states of monoclinic and tetragonal hafnia. The dashed and solid lines refer to the monoclinic and tetragonal polymorphs, respectively.

and end at the A point passing through M, X, Γ , Z, and R [see Fig. 4(b)]. We will compare theoretical values of the Raman and IR active modes to available experiment later in the paper. The inclusion of the long-range correction mostly influences the modes close to the Γ point as can be seen in Fig. 4(c). So in the total density of states (DOS) shown in Fig. 5 for two hafnia polymorphs the long-range correction is omitted. The phonon DOS is obtained by diagonalizing the dynamical matrix $D(\vec{k})$ on a dense $24 \times 24 \times 24$ special k -point grid over the entire first BZ. In Fig. 5 the solid and dashed lines show the density of states for tetragonal and monoclinic phases, respectively. The DOS of the monoclinic phase is blueshifted with respect to that of the tetragonal phase. Both spectra may be roughly divided into two regions: the low frequency part (below 350 cm^{-1}) and the high frequency part. In the case of monoclinic hafnia two parts are separated by a quasigap. The origin of this separation will be discussed later.

The transition temperature can now be calculated using simple thermodynamic analysis. Free energies of two phases are equal at the transition temperature. In the harmonic approximation (ignoring other forms of disorder), free energy of a system is given by

$$F_{Gibbs} = E + pV - TS = E_g + pV + E_{phonon} - TS_{phonon}. \quad (2)$$

The first term E_g is the internal energy of the ground state of HfO_2 obtained from *ab initio* calculations. The second term is negligible because the solid transformation discussed here occurs under ambient pressure and the volume change during the transformation is small. The last two terms together constitute the phonon contribution to free energy and can be calculated from the phonon density of states as follows:⁵⁷

$$F_{harm} = rk_B T \int_0^\infty g(\omega) \ln \left[2 \sinh \left(\frac{\hbar \omega}{2k_B T} \right) \right] d\omega, \quad (3)$$

where r is the number of atoms in the unit cell, ω is the phonon frequency, and $g(\omega)$ is the phonon DOS. In Fig. 6 we

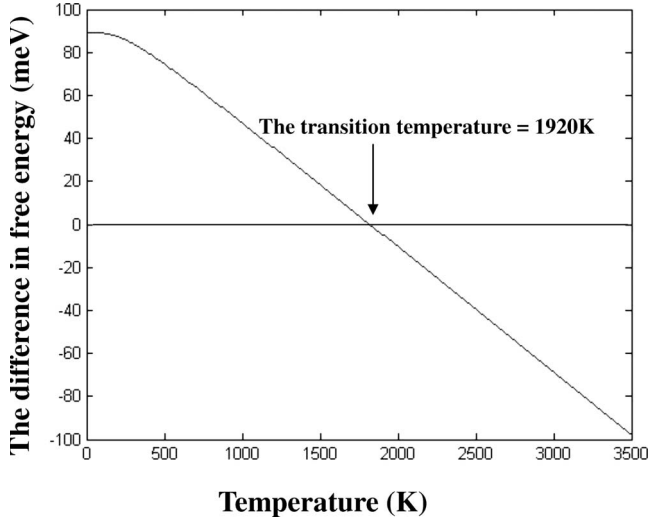


FIG. 6. The excess free energy of tetragonal HfO_2 with respect to the monoclinic phase $\Delta F = F_t - F_m$ as function of temperature ΔF changes its sign at $T_c = 1920$ K.

plot the difference in free energy per HfO_2 f.u. between the monoclinic and tetragonal phases. At the transition temperature the difference in entropy between two phases cancels the difference in the total energy, and the free energy difference is zero. From Fig. 6 it follows that the monoclinic phase is stable in the low temperature region when the E_g term dominates. Above 1920 K the tetragonal phase becomes more stable as its free energy is lower. Recently, Parlinski *et al.*,⁵⁸ using a similar approach, calculated the MT transition temperature for ZrO_2 to be about 1560 K. Considering the high temperature of these transitions and the use of the harmonic approximation the agreement with experiment is rather good as can be seen from Table II.

The heat capacity can be calculated as follows:⁵⁷

$$C_v(T) = \frac{1}{4k_B T^2} \int_0^\infty d\omega g(\omega) \frac{\hbar^2 \omega^2}{\sinh^2\left(\frac{\hbar\omega}{2k_B T}\right)}. \quad (4)$$

To compare the heat capacity of HfO_2 and ZrO_2 , we calculate the total density of states of monoclinic HfO_2 and ZrO_2 as shown in Fig. 7. The constant volume specific heat (C_v) of HfO_2 and ZrO_2 calculated using Eq. (4) is plotted in Fig. 8(a) for monoclinic phase and in Fig. 8(d) for tetragonal phase, respectively. In Figs. 8(b) and 8(c) we compare our calculations with the experimental data.^{11,48,53} In the case of zirconia the agreement with experiment is again very good at least in the low temperature regime when the harmonic approximation is expected to work well. The agreement is less impressive in the case of hafnia; however, the experimental data⁴⁸ are rather old and do not extend down to liquid helium temperature. An interesting feature of our calculation is a crossover at 190 K when C_v of zirconia becomes larger than that of hafnia. As we discuss later, the crossover can be attributed to the features in the phonon density of states and traced down to the interplay between the force constant and atomic mass.

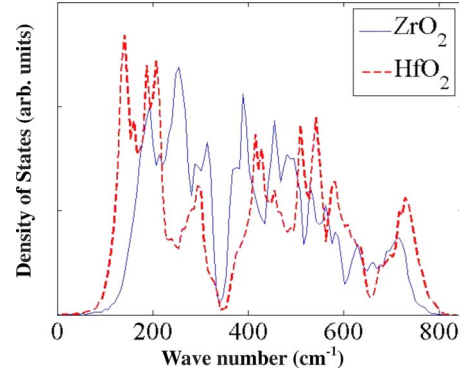


FIG. 7. (Color online) The phonon densities of states of monoclinic zirconia and hafnia. The dashed line and solid lines refer to the monoclinic hafnia and monoclinic zirconia, respectively.

VII. MINIMUM ENERGY PATH FOR THE MONOCLINIC TO TETRAGONAL TRANSFORMATION

Solid-solid phase transitions are divided into two broad categories, diffusional and diffusionless, depending on whether or not long-range atomic migration is involved.^{59,60} According to Cohen *et al.*,⁵⁹ diffusionless transformations can be further subdivided into two major categories, (i) transformations involving no macroscopic strain and (ii) lattice-distortive transformations involving macroscopic strain of the lattice. Further the lattice-distortive transformations having certain crystallographic characteristics are called martensitic transformations. The two phases involved in a martensitic transformation should have (1) a lattice correspondence and orientation relationship, (2) a strain invariant plane, and (3) an atom to atom correspondence.⁶⁰ One may choose to further classify martensitic transitions as either “proper” martensitic transformations, where a group-subgroup relationship exists between the symmetry groups of the parent and product phases,^{61,62} or as “reconstructive” martensitic transformations, where no such group-subgroup relationship exists.^{63,64} The MT transformations in ZrO_2 and HfO_2 are believed to be martensitic,^{12,60,65} however, the details such as the transition path from the monoclinic to the tetragonal phase or whether the transition is proper are not known.

To explore the connection between the tetragonal and monoclinic phases we turn to transition state theory. We need to establish the potential energy surface (PES) and identify the MEP describing the transformation. Since martensitic transformations include both the unit cell deformation (strain) and change of the internal coordinates (“shuffle”), the PES and MEP are functions of the internal atomic coordinates as well as of the unit cell lattice vectors. In order to follow the transformation a unit cell common to both phases needs to be chosen. This establishes the so-called lattice correspondence between the two phases. The set of lattice vectors (in Å) for a 12-atom primitive unit cell of the monoclinic phase is

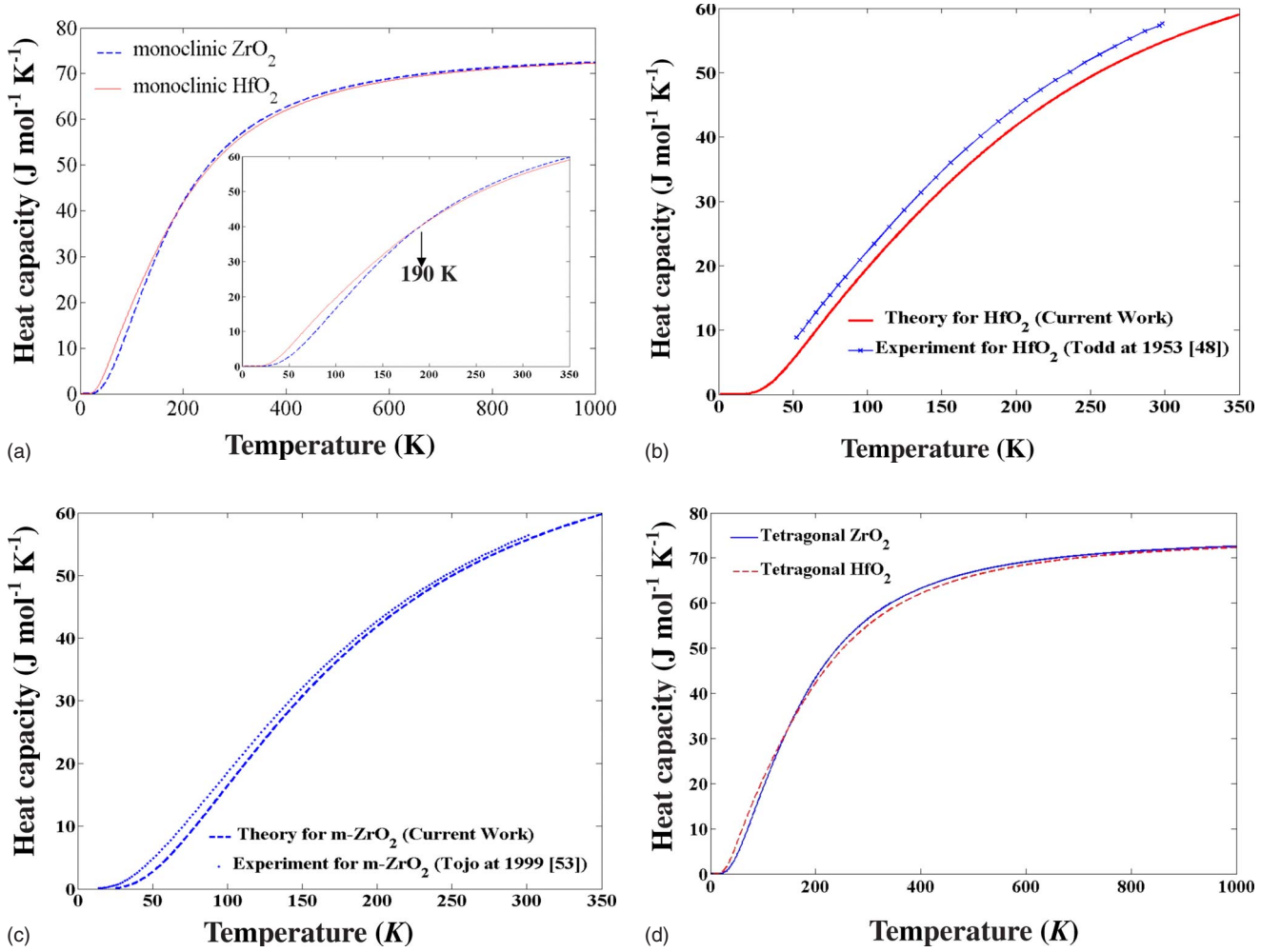


FIG. 8. (Color online) (a) The calculated heat capacity of monoclinic HfO₂ and ZrO₂ from 0 to 1000 K. In the embedded figure the crossover region is enlarged. (b) Experimental data for monoclinic hafnia are compared to our theoretical results from 0 to 350 K. (c) Experimental data for monoclinic zirconia are compared to our theoretical results from 0 to 350 K. (d) The calculated heat capacity of tetragonal HfO₂ and ZrO₂ from 0 to 1000 K.

$$\eta_m = \begin{pmatrix} 5.0258 & 0.0000 & 0.0000 \\ 0.0000 & 5.1323 & 0.0000 \\ -0.8616 & 0.0000 & 5.1109 \end{pmatrix} \begin{matrix} \cdots \cdots a_m \\ \cdots \cdots b_m \\ \cdots \cdots c_m \end{matrix}, \quad (5)$$

where a_m , b_m , and c_m represent the three axes of the primitive cell of the monoclinic phase. Similarly, the set of the primitive unit cell vectors of the tetragonal phase is

$$\eta_t = \begin{pmatrix} 3.5214 & 0.0000 & 0.0000 \\ 0.0000 & 3.5214 & 0.0000 \\ 0.0000 & 0.0000 & 5.0773 \end{pmatrix}. \quad (6)$$

However, there are only six atoms in this cell. To establish the one-to-one lattice correspondence between the monoclinic and tetragonal cells, instead of a primitive cell we use a $\sqrt{2}$ -doubled cell for the tetragonal phase. The new cell vector set is

$$\eta_t = \begin{pmatrix} 4.9800 & 0.0000 & 0.0000 \\ 0.0000 & 4.9800 & 0.0000 \\ 0.0000 & 0.0000 & 5.0773 \end{pmatrix} \begin{matrix} \cdots \cdots a_t \\ \cdots \cdots b_t \\ \cdots \cdots c_t \end{matrix}. \quad (7)$$

There are 12 atoms in this cell, same as in the monoclinic one. During the monoclinic to tetragonal transformation there are three possible lattice orientation schemes (LOSs) A, B, and C depending on which monoclinic axis a_m , b_m , or c_m is parallel to c_t as shown in Table V.⁶⁰ Bailey studied the LOS by transmission electron microscopy and found direct

TABLE V. Possible lattice correspondence schemes between monoclinic and tetragonal cells.

Lattice correspondence			
LC A	$a_t \rightarrow b_m$	$b_t \rightarrow c_m$	$c_t \rightarrow a_m$
LC B	$a_t \rightarrow a_m$	$b_t \rightarrow c_m$	$c_t \rightarrow b_m$
LC C	$a_t \rightarrow a_m$	$b_t \rightarrow b_m$	$c_t \rightarrow c_m$

TABLE VI. The fractional atomic coordinates of tetragonal hafnia in the $\sqrt{2}$ doubled cell.

	X	Y	Z
Oxygen atom 1	0.250	0.250	0.206
Oxygen atom 2	0.750	0.750	0.206
Oxygen atom 3	0.750	0.250	0.794
Oxygen atom 4	0.250	0.750	0.794
Oxygen atom 5	0.250	0.250	0.706
Oxygen atom 6	0.750	0.750	0.706
Oxygen atom 7	0.750	0.250	0.294
Oxygen atom 8	0.250	0.750	0.294
Hafnium atom 9	0.000	0.000	0.000
Hafnium atom 10	0.000	0.500	0.500
Hafnium atom 11	0.500	0.000	0.500
Hafnium atom 12	0.500	0.500	0.000

evidence for an orientation relationship consistent with the LOS C,⁶⁰ more recently Simeone *et al.* used neutron diffraction, and their data supports the LOS B.⁶² Because the transmission electron microscopy is a direct method we adopt the LOS C scheme in this paper.

Experiments^{12,65} suggest that during the monoclinic to tetragonal transformation in zirconia the atoms retain their neighbors in both phases (making it a proper martensitic transformation). Therefore, we postulate the atom correspondence leading to the minimal atomic movement in both HfO_2 and ZrO_2 and find one-to-one correspondence between the atoms of the tetragonal and monoclinic phases (see Tables VI and VII). In order to satisfy the condition of minimal atomic movement we shift the cell of the monoclinic phase to have a metal atom at the origin. We write the fractional atomic coordinates in monoclinic and tetragonal phases as $\{v_m^{i,\alpha}\}$ and $\{v_t^{i,\alpha}\}$, where i corresponds to the atom number (see Tables VI and VII) and $\alpha=x, y, z$.

In principle, the PES is a function of nine parameters describing the unit cell and 36 additional parameters describing the atomic positions. To simplify the picture we adopt the following approximation. The lattice distortion accompany-

TABLE VII. The fractional atomic coordinates of monoclinic hafnia.

	X	Y	Z
Oxygen atom 1	0.278	0.200	0.309
Oxygen atom 2	0.647	0.615	0.457
Oxygen atom 3	0.799	0.115	0.627
Oxygen atom 4	0.170	0.700	0.774
Oxygen atom 5	0.278	0.218	0.809
Oxygen atom 6	0.650	0.803	0.957
Oxygen atom 7	0.799	0.303	0.127
Oxygen atom 8	0.170	0.718	0.274
Hafnium atom 9	0.002	0.002	0.000
Hafnium atom 10	0.002	0.417	0.500
Hafnium atom 11	0.446	-0.084	0.584
Hafnium atom 12	0.446	0.502	0.084

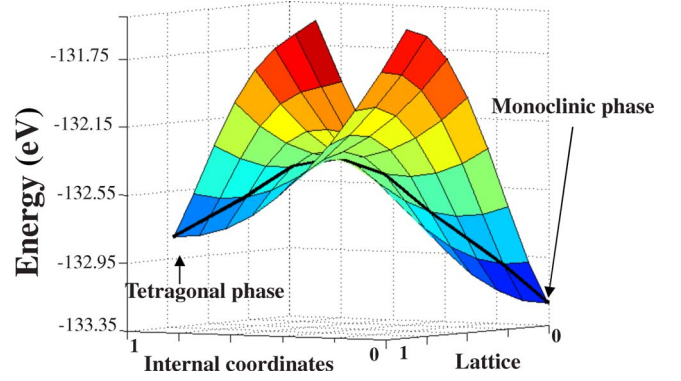


FIG. 9. (Color online) The potential energy surface during the tetragonal to monoclinic phase transformation. The minimum energy pathway (thick black line) between two phases indicates a 0.22 eV/mol barrier for the tetragonal to monoclinic phase transition.

ing the phase transition is rather small, and we assume a uniform transformation of the lattice vectors. Furthermore, in the spirit of the minimal atomic movement we also assume a uniform transformation of the atomic coordinates. We now can write the energy as a function of two parameters,

$$E(x, y) = E(\{\eta_x\}, \{v_y\}). \quad (8)$$

Here x and y are defined from the interpolation relations where $\eta_x = (1-x)\eta_m + x\eta_t$ is the lattice vector set and $v_y^{i,\alpha} = (1-y)v_m^{i,\alpha} + yv_t^{i,\alpha}$ are the fractional atomic coordinates describing the state of a system between two end phases; in this picture x and y change from 0 to 1, 0 and 1 being the monoclinic and tetragonal phase sets, respectively. Using these parameters as two independent variables we map the PES of hafnia and zirconia in two dimensions as shown in Fig. 9. We identify the MEP on the energy surface thus generated, shown as a thick black curve in Fig. 9. One can clearly see the saddle point (the transition state) at the top of the MEP. The symmetry of the transition state is $P2_1/c$ (same as in the monoclinic phase). The transition barrier is equal to the energy difference between the monoclinic phase and the saddle point. We find the barrier in hafnia to be 20.3 kJ/mol (0.21 eV per HfO_2 molecule) and that in zirconia to be 16.3 kJ/mol (0.17 eV per ZrO_2 molecule). The ratio of the barrier heights is close to the ratio of transition temperatures of hafnia and zirconia (see Table II). Here it is worth mentioning that we find no barrier for the transition between the cubic and tetragonal phases that will be discussed in a separate paper.

VIII. COMPARISON OF ZIRCONIA AND HAFNIA

As group IVB metals both zirconium and hafnium have the same valence configuration—two d electrons and two s electrons—which explains the many similarities in their chemistry. Their corresponding dioxides zirconia and hafnia crystallize in the same three phases (Fig. 1). The lattice parameters are rather similar as can be seen in Table III, owing to similar ionic radii which reflect the so-called lanthanide contraction.⁶⁶ Theoretically (see Table III), we find zirconia to have a slightly larger vol/f.u. than hafnia. Experimentally,

TABLE VIII. Experimental Raman spectra (Ref. 67) of the monoclinic phases of ZrO₂ and HfO₂ (band intensity: s—strong, m—medium, and w—weak).

No.	Experiments		
	HfO ₂	ZrO ₂	HfO ₂ /ZrO ₂
1	774 (s)	757	1.02
2	642 (s), B _g	616	1.04
3	672 (s), A _g	637	1.05
4	580 (m), A _g	556	1.04
5	552 (m), B _g	536	1.03
6	522 (m), B _g	505	1.03
7	500 (vs), A _g	476	1.05
8	398 (s)	385	1.03
9	384 (s), B _g	381	1.01
10	336 (s), A _g	348	0.97
11	256 (s), B _g	334	0.78
12	270 (m), A _g	305	0.88
13	242 (m)	270	0.9
14	168 (m), B _g	224	0.75
15	150 (m), A _g	190	0.79
16		179	
17	135 (s), A _g	179	0.75
18	108/83 (s), A _g	102	1.06/0.82

this is the case for the monoclinic phase but is reversed for the tetragonal phase. However, the measurements for the tetragonal phase of the two materials are done at different temperatures since the MT transition temperature in hafnia is 30% higher than that in zirconia, and the tetragonal phase is not quenchable to room temperature, while the calculations correspond to 0 K for both materials. Both MT and TC phase transitions in hafnia take place at much higher temperature than in zirconia. Vibrational spectra of monoclinic HfO₂ and ZrO₂ have been recently examined by Raman spectroscopy by Quintard *et al.*⁶⁷ We show their results in Table VIII. The

TABLE IX. Calculated Γ -point phonon frequencies classified according to irreducible representations of symmetry group C_{2h} of monoclinic hafnia. A_g and B_g modes are Raman active, while A_u and B_u modes are IR active.

	Wave number (cm ⁻¹) of A _g (Raman active modes)			Wave number (cm ⁻¹) of B _g (Raman active modes)			Wave number (cm ⁻¹) of A _u (IR)		Wave number (cm ⁻¹) of B _u (IR)	
	HfO ₂	ZrO ₂	HfO ₂ /ZrO ₂	HfO ₂	ZrO ₂	HfO ₂ /ZrO ₂	HfO ₂	ZrO ₂	HfO ₂	ZrO ₂
1	695.9	629.71	1.105	785.47	747.8	1.050	675.89	643.32	752.02	712.15
2	600.74	552.22	1.088	663.23	612.9	1.082	632.1	574.12	540.87	493.73
3	511.5	453.88	1.127	577.91	538.11	1.074	521.11	475.86	429.97	429.79
4	409.83	388.41	1.055	536.67	481.38	1.115	439.17	404.31	356.76	370.26
5	361	359.19	1.005	421.23	389.1	1.083	382.72	364.68	331.56	326.87
6	257.01	334.09	0.769	338.86	331.95	1.021	260.91	264.1	263.3	321.73
7	153.34	194.39	0.789	245.84	319.09	0.770	185.57	234.53	241.66	232.14
8	140.59	184.32	0.763	170.86	224.11	0.762	139.76	182.73	0	0
9	133.29	133.46	0.999	135.85	176.3	0.771	0	0	0	0

Raman mode frequencies in ZrO₂ are slightly lower than those of HfO₂ in the high frequency region (above 350 cm⁻¹). However, in the low frequency region, the frequencies of ZrO₂ are about 10–25 % higher than those of HfO₂. The results of our calculations of Raman modes of monoclinic HfO₂ and ZrO₂ are summarized in Table IX. Our results agree well with the previous calculation of hafnia.¹⁹ Theoretically we find a similar trend in mode frequencies when comparing the two oxides. Naively one would expect the vibrational spectrum of hafnia to be redshifted with respect to that of zirconia because of a larger atomic mass of hafnium (for a simple harmonic oscillator we have $\omega = \sqrt{k/m}$, where k is the spring constant and m is the mass). However, the picture is more complicated. Our *ab initio* calculations reveal that the magnitude of the interatomic force constants in zirconia is approximately 10% smaller than that in hafnia. In Fig. 10 we compare the effective force constants for both materials by plotting the absolute values of the dynamical matrix at the Γ point without including the mass factor (we plot $|\sum_m B(0, \mu; m, \nu)|$, where B is the force constant coupling an atom μ in the central cell with an atom ν in the m th cell). The highest value in hafnia is almost 200 eV/Å², while in zirconia it is only 160 eV/Å². This would suggest a blueshift of the hafnia spectrum. However, for the actual frequency calculation (diagonalization of the dynamical matrix) the force constant matrix is “renormalized” by the mass factor as follows:

$$\mathbf{D}^0(\mathbf{k}; \mu\nu) = \frac{1}{\sqrt{M_\mu M_\nu}} \sum_m \mathbf{B}(0, \mu; \mathbf{m}, \nu) \times \exp\{-2\pi i \cdot [\mathbf{R}(0, \mu) - \mathbf{R}(\mathbf{m}, \nu)]\}. \quad (9)$$

In Fig. 11 we show relative amplitudes of the atomic movement in all vibration modes of monoclinic hafnia at the Γ point. It is clearly seen that the low frequency modes correspond to the movement involving predominantly metal atoms. The mass ratio between Hf and Zr is approximately 2. In other words, even though the force constant is smaller in zirconia, the dynamical matrix is enhanced by the mass factor in the low frequency range. In the high frequency region,

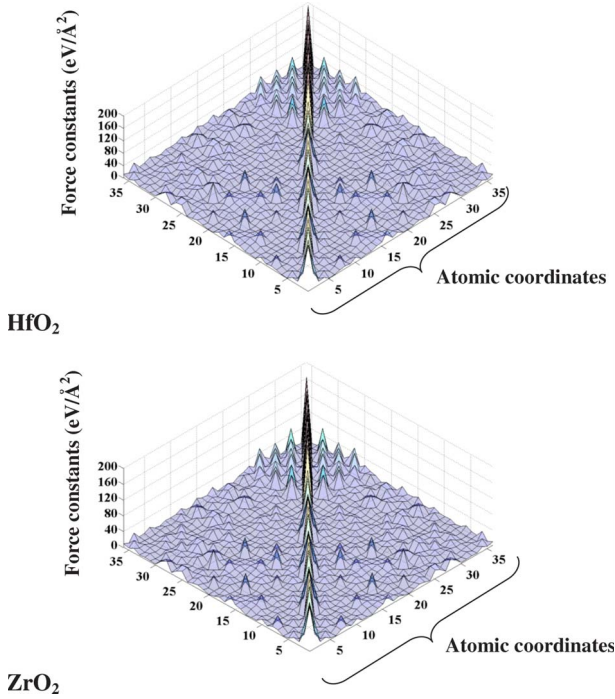


FIG. 10. (Color online) The 36×36 force constant matrices of HfO_2 and ZrO_2 in $\text{eV}/\text{\AA}^2$. The first 24×24 block corresponds to oxygen atoms, and the 12×12 diagonal block starting with row 25 corresponds to metal atoms Hf or Zr.

the vibrational modes are associated with the movement of oxygen atoms (Fig. 11). Thus in both hafnia and zirconia the mass factors are the same, and the frequency is controlled by the force constant. Due to weaker force constants of zirconia, its high frequency modes have frequencies lower than those of hafnia. This is true beyond the Γ point as can be seen in the DOS plots in Fig. 7. Also, we can attribute the spectral gap at around 350 cm^{-1} in the phonon density of states for both hafnia and zirconia to the transition from the metal-dominated modes to oxygen dominated ones.

We have shown that in the low frequency region the phonon modes of zirconia have higher frequencies than those of hafnia. This result has peculiar implications for thermodynamic properties of two oxides. The heat capacity of zirconia should be smaller than that of hafnia at low temperature because only low frequency modes can be excited. On the other hand, at high temperature the heat capacity of zirconia should be larger than that of hafnia because in the high frequency region zirconia has higher frequency modes. As shown in Fig. 8(a) we find that the heat capacity of monoclinic HfO_2 crosses that of monoclinic ZrO_2 at 190 K. The result should not be seriously affected by the validity of the harmonic approximation because of the relatively low temperature of the crossover. There are several experimental measurements of the enthalpy and heat capacity of monoclinic zirconia^{11,53} which are in good agreement with our calculations. However, we have found only one experimental report of the heat capacity of hafnia dating back to 1953 and extending down below liquid nitrogen temperature.⁴⁸ We plan to measure the heat capacity of hafnia at 4–300 K using modern calorimetric methodology.

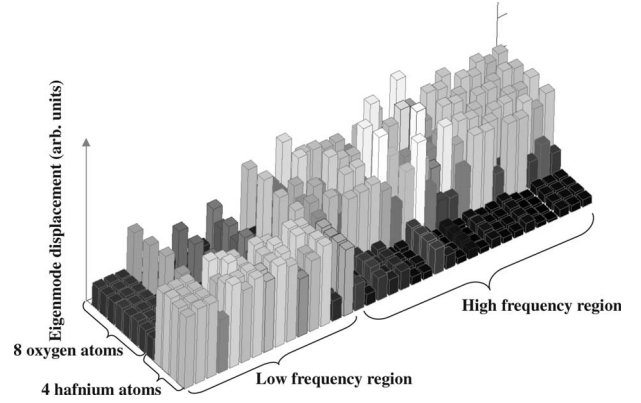


FIG. 11. The bar plot of 36 eigenmodes of Γ point of monoclinic HfO_2 . The height denotes the displacement of one atom in an eigenmode. There are 12 points in the x axis representing 12 atoms in the primitive unit. The 36 modes are arranged in the ascending order of frequency along the y axis.

IX. CONCLUSIONS

We have investigated the monoclinic to tetragonal phase transition in hafnia using a combination of first-principles calculations and differential thermal analysis. We find the transition enthalpy to be about 9 kJ/mol and good agreement of theory and experiment. We propose a theory of the phase transition and calculate the minimum energy path from a high symmetry tetragonal to a lower symmetry monoclinic phase. With this theory we are able to estimate the transition barriers in hafnia and zirconia to be 20.3 and 16.3 kJ/mol, respectively. We analyzed vibrational spectra of hafnia and zirconia and using group theory identified Raman and IR active modes. The frequencies are in good agreement with reported experiment. Despite the two oxides being very similar we find subtle differences in the phonon spectra. The force constants in zirconia are calculated to be about 10% lower than those in hafnia, which results in a blueshift of hafnia modes with respect to zirconia modes in the high frequency range. However, in the low frequency range (below 350 cm^{-1}) the mass factor cancels the force constant and hafnia modes are redshifted. Based on our detailed theoretical analysis of the phonon spectra we calculated the temperature dependence of specific heat in both oxides. Theoretical results agree well with heat capacity data available for zirconia, and we plan new measurements for hafnia. We also predict a crossover at 190 K with specific heat of zirconia exceeding that of hafnia. We plan to test these predictions by measuring the low temperature heat capacity of hafnia using modern calorimetric techniques at 4–200 K experimentally in a future study.

ACKNOWLEDGMENTS

This work was supported by the National Science Foundation under Grant No. DMR-0606464 and Texas Advanced Computing Center. We thank John Ekerdt and Tuo Wang for insightful discussions.

*demkov@physics.utexas.edu

- ¹2007 International Technology Roadmap for Semiconductors, Semiconductor Industry Association, San Jose, 2007.
- ²G. D. Wilk, R. M. Wallace, and J. M. Anthony, *J. Appl. Phys.* **89**, 5243 (2001).
- ³P. S. Lysaght, J. C. Woicik, M. A. Sahiner, B. H. Lee, and R. Jammy, *Appl. Phys. Lett.* **91**, 122910 (2007).
- ⁴X. Luo, A. A. Demkov, D. Triyoso, P. Fejes, R. Gregory, and S. Zollner, *Phys. Rev. B* **78**, 245314 (2008).
- ⁵A. A. Demkov, J. Ortega, O. F. Sankey, and M. P. Grumbach, *Phys. Rev. B* **52**, 1618 (1995).
- ⁶D. Ceresoli and D. Vanderbilt, *Phys. Rev. B* **74**, 125108 (2006).
- ⁷M. F. Trubelja, *Ionic Conductivity in the Hafnia-Rare Earth Systems and Phase Equilibria in the System Hafnia-Zirconia-Yttria* (Pennsylvania State University, University Park, 1987).
- ⁸Y. Ishibashi and V. Dvorak, *J. Phys. Soc. Jpn.* **58**, 4211 (1989).
- ⁹J. Chevalier, L. Gremillard, A. V. Virkar, and D. R. Clarke, *J. Am. Ceram. Soc.* **92**, 1901 (2009).
- ¹⁰C. Wang, M. Zinkevich, and F. Aldinger, *J. Am. Ceram. Soc.* **89**, 3751 (2006).
- ¹¹Y. Moriya and A. Navrotsky, *J. Chem. Thermodyn.* **38**, 211 (2006).
- ¹²R. N. Patil and E. C. Subbarao, *Acta Crystallogr.* **26**, 535 (1970).
- ¹³F. Frey, H. Boysen, and T. Vogt, *Acta Crystallogr., Sect. B: Struct. Sci.* **46**, 724 (1990).
- ¹⁴O. Ohtaka, H. Fukui, T. Kunisada, T. Fujisawa, K. Funakoshi, W. Utsumi, T. Irifune, K. Kuroda, and T. Kikegawa, *J. Am. Ceram. Soc.* **84**, 1369 (2001).
- ¹⁵H. L. Schick, *Thermodynamics of Certain Refractor Compounds, Thermodynamic Tables, Bibliography, and Property File Vol. II* (Academic Press, New York, 1966), Secs. VII–IX.
- ¹⁶I. Barin, O. Knacke, and O. Kubaschewski, *Thermochemical Properties of Inorganic Substances* (Springer-Verlag, Berlin, 1977).
- ¹⁷R. L. Orr, *J. Am. Chem. Soc.* **75**, 1231 (1953).
- ¹⁸C. D. Pears, *The Thermal Properties of Twenty-Six Solid Materials To 5000 F or Their Destruction Temperatures* (Southern Research Institute, Birmingham, AL, 1963).
- ¹⁹X. Y. Zhao and D. Vanderbilt, *Phys. Rev. B* **65**, 233106 (2002).
- ²⁰M. Sternik and K. Parlinski, *J. Chem. Phys.* **122**, 064707 (2005).
- ²¹J. E. Jaffe, R. A. Bachorz, and M. Gutowski, *Phys. Rev. B* **72**, 144107 (2005).
- ²²G. M. Rignanese, F. Detraux, X. Gonze, and A. Pasquarello, *Phys. Rev. B* **64**, 134301 (2001).
- ²³M. Smirnov, A. Mirgorodsky, and R. Guinebretière, *Phys. Rev. B* **68**, 104106 (2003).
- ²⁴D. Muñoz Ramo, A. L. Shluger, and G. Bersuker, *Phys. Rev. B* **79**, 035306 (2009).
- ²⁵H. Ozturk and M. Durandurdu, *Phys. Rev. B* **79**, 134111 (2009).
- ²⁶G. Kresse and J. Furthmüller, *Phys. Rev. B* **54**, 11169 (1996).
- ²⁷D. Vanderbilt, *Phys. Rev. B* **41**, 7892 (1990).
- ²⁸H. J. Monkhorst and J. D. Pack, *Phys. Rev. B* **13**, 5188 (1976).
- ²⁹J. P. Coughlin and E. G. King, *J. Am. Chem. Soc.* **72**, 2262 (1950).
- ³⁰S. H. Tsagareishvili, *Russ. J. Inorg. Chem.* **10**, 171 (1965).
- ³¹V. A. Kirillin, A. E. Sheindlin, V. Y. Chekhovskoi, I. A. Zhukova, and V. D. Tarasov, *Teplofiz. Vys. Temp.* **4**, 878 (1966).
- ³²V. Y. Chekhovskoi and V. D. Tarasov, *Teplofiz. Vys. Temp.* **17**, 754 (1979).
- ³³M. Yashima, T. Mitsuhashi, H. Takashina, M. Kakihana, T. Ikegami, and M. Yoshimura, *J. Am. Ceram. Soc.* **78**, 2225 (1995).
- ³⁴D. A. Jerebtsov, G. G. Mikhailov, and S. V. Sverdina, *Ceram. Int.* **27**, 247 (2001).
- ³⁵A. Suresh, M. J. Mayo, and W. D. Porter, *J. Mater. Res.* **18**, 2912 (2003).
- ³⁶R. J. Ackermann, E. G. Rauh, and C. A. Alexander, *High. Temp. Sci.* **7**, 304 (1975).
- ³⁷Y. Du, Z. P. Jin, and P. Y. Huang, *J. Am. Ceram. Soc.* **75**, 3040 (1992).
- ³⁸P. Liang, N. Dupin, S. G. Fries, H. J. Seifert, I. Ansara, H. L. Lukas, and F. Aldinger, *Z. Metallkd.* **92**, 747 (2001).
- ³⁹R. Arroyave, L. Kaufman, and T. W. Eagar, *CALPHAD: Comput. Coupling Phase Diagrams Thermochem.* **26**, 95 (2002).
- ⁴⁰M. Chen, B. Hallstedt, and L. J. Gauckler, *Solid State Ionics* **170**, 255 (2004).
- ⁴¹M. W. Pitcher, S. V. Ushakov, A. Navrotsky, B. F. Woodfield, G. S. Li, J. Boerio-Goates, and B. M. Tissue, *J. Am. Ceram. Soc.* **88**, 160 (2005).
- ⁴²P. K. Schelling, S. R. Phillpot, and D. Wolf, *J. Am. Ceram. Soc.* **84**, 1609 (2001).
- ⁴³A. Navrotsky, L. Benoist, and H. Lefebvre, *J. Am. Ceram. Soc.* **88**, 2942 (2005).
- ⁴⁴I. Molodetsky and A. Navrotsky, *Z. Phys. Chemie-Int. J. Res. Phys. Chem. Chem. Phys.* **207**, 59 (1998).
- ⁴⁵T. A. Lee, A. Navrotsky, and I. Molodetsky, *J. Mater. Res.* **18**, 908 (2003).
- ⁴⁶P. Simoncic and A. Navrotsky, *J. Mater. Res.* **22**, 876 (2007).
- ⁴⁷T. A. Lee and A. Navrotsky, *J. Mater. Res.* **19**, 1855 (2004).
- ⁴⁸S. S. Todd, *J. Am. Chem. Soc.* **75**, 3035 (1953).
- ⁴⁹J. Adam and M. D. Rodgers, *Acta Crystallogr.* **12**, 951 (1959).
- ⁵⁰J. Wang, H. P. Li, and R. Stevens, *J. Mater. Sci.* **27**, 5397 (1992).
- ⁵¹J. S. Arthur, *J. Appl. Phys.* **21**, 732 (1950).
- ⁵²M. V. Nevitt, Y. Fang, and S. K. Chan, *J. Am. Ceram. Soc.* **73**, 2502 (1990).
- ⁵³T. Tojo, T. Atake, T. Mori, and H. Yamamura, *J. Chem. Thermodyn.* **31**, 831 (1999).
- ⁵⁴H. Tanaka, S. Sawai, K. Morimoto, and K. Hisano, *J. Therm. Anal. Calorim.* **64**, 867 (2001).
- ⁵⁵C. Degueldre, P. Tissot, H. Lartigue, and M. Pouchon, *Thermochim. Acta* **403**, 267 (2003).
- ⁵⁶G. K. Horton and A. A. Maradudin, *Dynamical Properties of Solids* (American Elsevier Publishing Co., New York, 1974).
- ⁵⁷N. W. Ashcroft and N. D. Mermin, *Solid State Physics* (Rinehart and Winston, New York, 1975).
- ⁵⁸K. Parlinski, Z. Q. Li, and Y. Kawazoe, *Phys. Rev. Lett.* **78**, 4063 (1997).
- ⁵⁹M. Cohen, G. B. Olson, and P. C. Clapp, *Proceedings of the International Conference of Martensitic Transformations: ICOMAT 1979* (MIT Press, Cambridge, MA, 1979), p. 1.
- ⁶⁰J. E. Bailey, *Proc. R. Soc. London, Ser. A* **279**, 359 (1964).
- ⁶¹D. M. Hatch, H. T. Stokes, and R. M. Putnam, *Phys. Rev. B* **35**, 4935 (1987).
- ⁶²K. Bhattacharya, *Theory of martensitic microstructure and the shape-memory effect*, 1998, <http://mechmat.caltech.edu/~bhatta/pdffiles/kbchap.pdf>
- ⁶³O. Tolaedano and V. Dmitriev, *Reconstructive Phase Transitions*

(World Scientific, Singapore, 1996).

⁶⁴H. T. Stokes, D. M. Hatch, J. J. Dong, and J. P. Lewis, Phys. Rev. B **69**, 174111 (2004).

⁶⁵G. M. Wolten, Acta Crystallogr. **17**, 763 (1964).

⁶⁶G. Wulfsberg, *Inorganic Chemistry* (University Science Books, Sausalito, CA, 2000).

⁶⁷P. E. Quintard, P. Barberis, A. P. Mirgorodsky, and T. Merle-Mejean, J. Am. Ceram. Soc. **85**, 1745 (2002).